RSC Advances

PAPER

View Article Online
View Journal | View Issue

Cite this: *RSC Adv.*, 2014, **4**, 58631

Source and major species of CH_x ($x = 1–3$) in acetic acid synthesis from methane–syngas on Rh catalyst: a theoretical study†

Xiaojun Zhao,[ab] Riguang Zhang,*[a] Qiang Wang,[b] Debao Li,[b] Baojun Wang*[a] and Lixia Ling[a]

Received 11th June 2014
Accepted 3rd October 2014

DOI: 10.1039/c4ra05591h

www.rsc.org/advances

Density functional calculations have been carried out to investigate the source and major species of CH_x ($x = 1–3$) involved in acetic acid synthesis from methane–syngas on the Rh(111) surface. All possible formation pathways of CH_x ($x = 1–3$) from methane and syngas have been systematically investigated. For CH_x formation from methane, our results show that CH is the most abundant species; for CH_x formation from syngas, all CH_x ($x = 1–3$) species form from CHO by CO hydrogenation, and the optimal formation routes of CH_x show that CH and CH_3 are the most abundant species rather than CH_2 and CH_3OH. On the other hand, CH formed by methane is more favourable than CH and CH_3 formed by syngas; meanwhile, CO insertion into CH_x species to form C_2 oxygenates as acetic acid precursors is more favourable than CO hydrogenation to CH and CH_3. As a result, in acetic acid synthesis from methane–syngas, CH_x ($x = 1–3$) species come from methane rather than syngas, and the corresponding primary species is CH. In addition, the CO in syngas is predominantly responsible for insertion reactions that produce CHCO, which is a C_2 oxygenate precursor leading to the formation of acetic acid. Furthermore, microkinetic modelling analysis shows that the major product of acetic acid synthesis from methane–syngas on the Rh(111) surface is CH_3COOH, and that the production of CH_3OH cannot compete with that of CH_3COOH.

1. Introduction

Acetic acid is an important commodity organic chemical used in a broad range of applications, such as the synthesis of chemical products as well as a raw material for pesticides, fertilisers, medicine and food industry products.[1,2] Due to the extensive sources of methane and syngas, acetic acid produced from methane–syngas has attracted growing interest for its great value in both academic and industrial fields.[3–5] To date, many studies have sought catalysts with high activity and selectivity toward acetic acid synthesis from methane–syngas.[6–14] Previous studies by Xu *et al.*[8,9] have suggested that Rh-based catalysts are promising candidates for C_2 oxygenate formation from syngas due to their catalytic versatility for both CO dissociation and the insertion of undissociated CO.

It has been reported that two key steps exist in C_2 oxygenate formation from syngas: one is the formation of CH_x species; the other is the growth of the C–C chain by CO insertion into CH_x species that are precursors to C_2 oxygenates.[15–17] For CH_x species involved in acetic acid synthesis, a large number of experimental studies have shown that CH_x species are very important intermediates that are responsible for acetic acid synthesis.[6–11] For example, in the synthesis of acetic acid from methane, Wang *et al.*[6,7] concluded from their experiments that acetic acid is mainly synthesised from CH_3 and CO insertion reactions, while CH_2 can also be converted to acetic acid. Xu *et al.*[8,9] proposed that acetate groups are formed through CO insertion into metal alkyl bonds based on experimental studies, in which they synthesised acetic acid from syngas. Based on ^{13}C NMR spectroscopy results, Taniguchi *et al.*[10] proposed that acetic acid is synthesised *via* the reaction of CH_3 and CO to form CH_3CO precursor intermediates. Asadullah *et al.*[11] studied acetic acid synthesis from CH_4 and CO on Ca catalysts and suggested that CO acts as a trapping agent for CH_3 to form acetyl radical, which forms acetic acid in a later process; meanwhile, they also confirmed the sources of CH_3 and COOH in acetic acid using ^{13}C NMR spectroscopy. Currently, although the source of CH_x ($x = 1–3$) species can be detected using isotopic tracing techniques

[a]*Key Laboratory of Coal Science and Technology of Ministry of Education and Shanxi Province, Taiyuan University of Technology, No. 79 Yingze West Street, Taiyuan 030024, Shanxi, P.R. China. E-mail: zhangriguang@tyut.edu.cn; wangbaojun@tyut.edu.cn; Fax: +86-351-6041237; Tel: +86-351-6018239*

[b]*State Key Laboratory of Coal Conversion, Institute of Coal Chemistry, Chinese Academy of Sciences, Taiyuan 030001, Shanxi, P.R. China*

† Electronic supplementary information (ESI) available: The descriptions of rate constant calculations and microkinetic modelling as well as the rate constants of the major elementary reactions (Table S1) involved in acetic acid synthesis from methane–syngas on the Rh(111) surface have been presented in detail. See DOI: 10.1039/c4ra05591h

and NMR-spectroscopy, the detailed formation mechanism of CH_x species is still debated, especially the speciation of CH_x intermediates that could not be identified experimentally. To date, theoretical calculations have been used as a powerful tool to study the mechanism and kinetics of typical reactions,[18–23] including density functional theory (DFT) studies on acetic acid synthesis.[12–14,24–26] However, among these studies, few have focused on the source and speciation of CH_x intermediates involved in the synthetic process. As a result, a detailed investigation on the mechanism of CH_x (x = 1–3) formation from methane and syngas at the molecular level will help us better understand the source and speciation of CH_x (x = 1–3).

In this study, the source and speciation of CH_x (x = 1–3) involved in acetic acid synthesis from methane–syngas on the Rh(111) surface have been systematically investigated using DFT calculations together with periodic slab models. All possible formation pathways of CH_x species have been considered, and the activation barriers and reaction energies of all elementary reactions have been obtained. Furthermore, the most favourable CH_x monomer has been obtained. The results of this work are expected to provide a better understanding of the catalytic reactivity of Rh catalysts toward CH_x formation from methane–syngas and clarify the source and major species of CH_x.

2. Computational details

2.1. Surface model

For metal Rh, the (111) surface is the most abundant surface[27] and has been widely employed to investigate the reaction mechanisms of C_2 oxygenate formation[15,16] as well as the adsorption of diverse atoms and molecules.[28–31] We have calculated the surface energies of the low index (111), (110), and (100) surfaces that are considered to be the basic structures of Rh particles; the surface energy of the Rh(*hkl*) surface in vacuum is defined as follows:[32,33]

$$E_{\mathrm{suf}} = \frac{E_{\mathrm{Rh}(hkl)} - E_{\mathrm{bulk}}}{2S_{\mathrm{Rh}(hkl)}}$$

Here, E_{suf} is the surface energy of the Rh(*hkl*) surface, $E_{\mathrm{Rh}(hkl)}$ and E_{bulk} are the total energy of the Rh(*hkl*) surface in vacuum and the bulk phase of Rh containing the same number of atoms as in the slab, respectively, and $S_{\mathrm{Rh}(hkl)}$ is the surface area of Rh(*hkl*).

Our results show that the Rh(111) surface has the lowest surface energy (0.79 eV per atom) compared to those of Rh(110) (1.58 eV per atom) and Rh(100) (1.08 eV per atom). Namely, the Rh(111) surface is the most stable face-centred cubic surface of close-packed Rh metal. Therefore, in this study, a Rh(111) surface cleaved from the experimental fcc crystal structure with a lattice parameter of 3.80 Å[28] is selected to model an Rh catalyst under realistic conditions. The model employed in our study consists of a periodic $p(3 \times 3)$ supercell containing four layers of Rh atoms. A 15 Å vacuum slab is inserted into the direction perpendicular to the surface in order to separate the periodically repeated slabs. In all calculations, Rh atoms in the top three layers and all absorbed species are allowed to relax, while the bottom layer is fixed at the bulk position. For the Rh(111) surface, there are four different adsorption sites: top, bridge, hcp and fcc (Fig. 1).

2.2. Calculation methods

The quantum-chemical periodic calculations are performed using the Vienna *ab initio* Simulation Package (VASP) code.[34,35] To describe all exchange and correlation effects, the generalised gradient approximation (GGA) proposed by Perdew–Wang (PW91)[36] is employed. The electron–ion interactions are described by the projector-augmented wave (PAW) method.[37,38] Forces below 0.01 eV $Å^{-1}$ for ions are used as the criterion for relaxation convergence. When the total energy and the band structure energy changes between the two electronic optimisation steps are both smaller than 5×10^{-6} eV, the relaxation of the electronic degrees of freedom is assumed to be converged. A plane wave basis set with a kinetic energy cutoff of 400 eV is employed for the valence electrons. The supercell is sampled by a $4 \times 4 \times 1$ *k*-points grid generated *via* the Monkhorst-Pack procedure.[15,39] Spin-polarised calculations have been carried out for the isolated atoms and molecules in a $10 \times 10 \times 10$ Å cubic unit cell with a single *k*-point.[39]

To study the minimum energy reaction pathways, the climbing-image nudged elastic band method (CI-NEB)[40,41] is employed to find saddle points between the known reactants and products, and the transition states are optimised using the dimer method.[42,43] The optimised transition state structures are considered converged when the forces on all atoms are less than 0.05 eV $Å^{-1}$ at the various degrees of freedom.

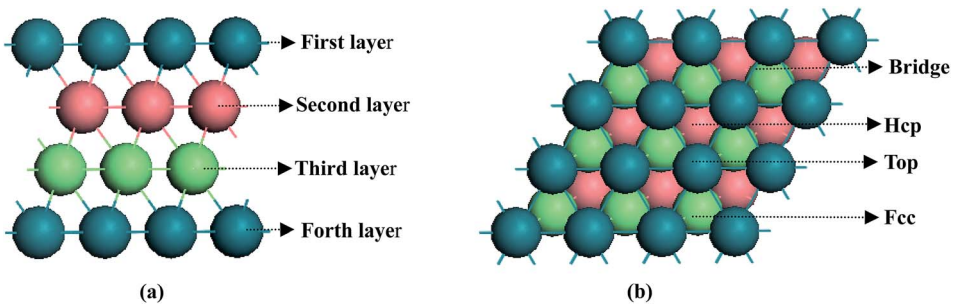

Fig. 1 Surface morphology and adsorption sites of the Rh(111) surface: (a) side view; and (b) top view.

For a reaction such as R (reactant) → P (product) on the Rh(111) surface, the reaction energy (ΔE) and activation barrier (E_a) are calculated according to the following formulas:

$$\Delta E = E_{P/Rh(111)} - E_{R/Rh(111)}$$

$$E_a = E_{TS/Rh(111)} - E_{R/Rh(111)}$$

where $E_{P/Rh(111)}$ and $E_{R/Rh(111)}$ are the total energies of the adsorbed product and reactant, respectively, and $E_{TS/Rh(111)}$ is the total energy of the transition state.

3. Results and discussion

3.1. Adsorption of reactants, products and possible intermediates

Adsorption energy, E_{ads}, is obtained using the expression $E_{ads} = E_{adsorbate} + E_{slab} - E_{adsorbate/slab}$, where $E_{adsorbate}$ is the total energy of free adsorbate in the gas phase, E_{slab} is the total energy of the bare slab, and $E_{adsorbate/slab}$ is the total energy of the optimised adsorbate-surface system. Thus, a more positive adsorption energy corresponds to a more stable binding system.

For the adsorption of all possible species involved in CH_x (x = 1–3) formation, four different sites on the Rh(111) surface are investigated. The most stable adsorption configurations obtained from our calculations are shown in Fig. 2.

C, H and O C prefers to adsorb at the hcp site, while H and O prefer to adsorb at the fcc site (Fig. 2(a–c), respectively), in agreement with previous DFT results.[29]

CO and OH CO prefers to adsorb at the hcp site *via* the C atom with the C–O bond perpendicular to the surface, as shown in Fig. 2(d). Similar to CO, OH is adsorbed at the fcc site *via* the O atom, as shown in Fig. 2(e).

CH, CH_2 and CH_3 CH and CH_2 prefer to adsorb at the hcp site *via* the C atom, as shown in Fig. 2(f and g). CH is adsorbed perpendicularly to the surface, while CH_2 is adsorbed asymmetrically at the hcp site. In contrast, CH_3 prefers to adsorb at the fcc site, as shown in Fig. 2(h), in agreement with the conclusions obtained by Xiao and Xie.[30]

CHO, CH_2O and CH_3O CHO, CH_2O and CH_3O all preferentially adsorb at the hcp site, as shown in Fig. 2(i–k). CHO presents the top(O)-bridge(C) configuration, while CH_2O prefers the top(C)-bridge(O) configuration. CH_3O prefers to adsorb through the O atom with the O–C bond perpendicular to the surface.

COH, CHOH and CH_2OH COH prefers to adsorb at the hcp site *via* the C atom with the O–H bond tilted relative to the surface, as shown in Fig. 2(l). CHOH preferentially adsorbs at the bridge site with the O–H bond pointing toward the surface, as shown in Fig. 2(m). CH_2OH prefers to adsorb at the top site through its C atom, the C–O bond is almost parallel to the surface, as shown in Fig. 2(n).

CH_4, CH_3OH and H_2O CH_4, CH_3OH and H_2O are all weakly adsorbed. CH_4 prefers to adsorb at the top site, as shown in Fig. 2(o). CH_3OH and H_2O prefer to locate at the top sites *via* O atoms, as shown in Fig. 2(p and q). For H_2O, the plane formed by the three atoms is nearly parallel to the surface; this result is in good agreement with the previous study by van Grootel *et al.*[44]

3.2. CH_x (x = 1–3) formation from methane

For CH_x (x = 1–3) formation from methane, the sequential dehydrogenation of CH_4 is investigated. The potential energy profiles of these reactions together with the structures of initial states (ISs), transition states (TSs) and final states (FSs) are displayed in Fig. 2 and 3.

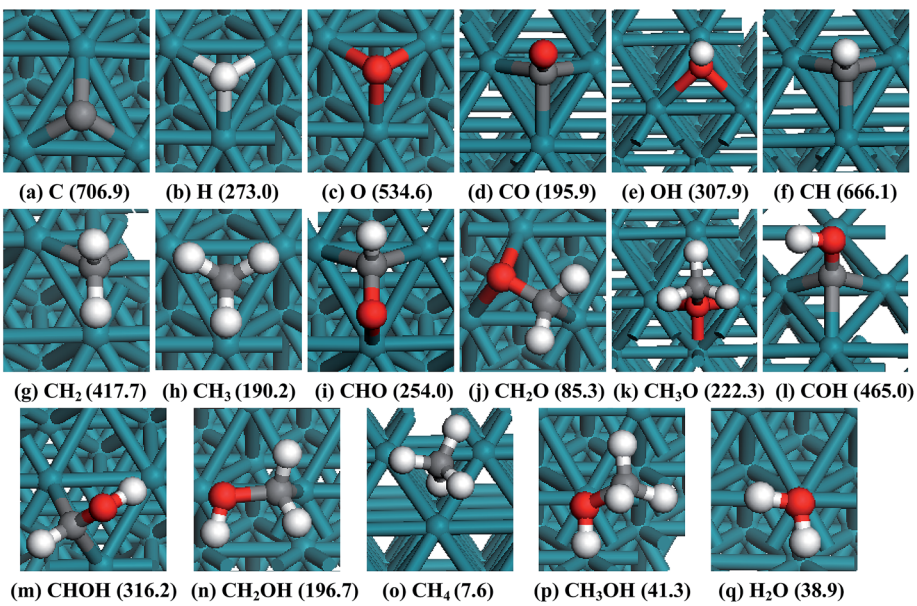

Fig. 2 The most stable adsorption configurations for all possible species involved in CH_x (x = 1–3) formation from methane and syngas on the Rh(111) surface. The Rh, C, H and O atoms are shown as green, grey, white and red balls, respectively. The energy unit is in kJ mol^{-1}.

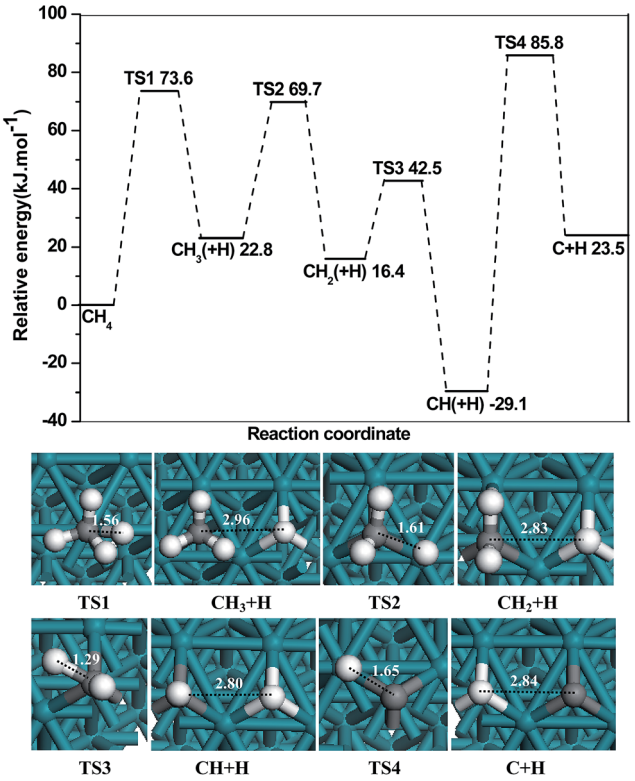

Fig. 3 The potential energy profile of CH_4 dehydrogenation to C together with the structures of initial states, transition states and final states. Bond lengths are in Å.

The elementary dehydrogenation reaction of CH_4 to CH_3 proceeds through a transition state TS1 to form CH_3 + H. In CH_3 + H, CH_3 and H are adsorbed at the adjacent fcc sites. The distance between the dissociated H atom and the C atom is elongated to 1.56 Å in TS1 and 2.96 Å in CH_3 + H. This elementary reaction needs to overcome an activation barrier of 73.6 kJ mol^{-1}, and it is found to be endothermic by 22.8 kJ mol^{-1}.

CH_3 dehydrogenates into CH_2 + H *via* TS2. In CH_2 + H, CH_2 and H are adsorbed at the adjacent hcp sites, the distance between dissociated H and C atoms is 2.83 Å. This elementary reaction has an activation barrier of 46.9 kJ mol^{-1} and it is exothermic by 6.4 kJ mol^{-1}.

For CH_2 dehydrogenation to CH, CH_2 adsorbs at the hcp site, and the dissociation products CH and H are located at the adjacent hcp site. This elementary reaction proceeds through a transition state TS3, in which the distance between the dissociated H and C atoms becomes 1.29 Å. This reaction is exothermic by 45.5 kJ mol^{-1} with a low activation barrier of only 26.1 kJ mol^{-1}.

Finally, CH dehydrogenates into C + H *via* TS4. In C + H, C and H are located at the adjacent hcp site, and the distance between C and H atoms is 2.84 Å. This elementary reaction is endothermic by 52.6 kJ mol^{-1}, and its activation barrier of 114.9 kJ mol^{-1} is significantly large compared to the other elementary reactions involved in CH_4 dehydrogenation.

We can see from Fig. 3 that during the CH_4 dissociation process, CH_2 can easily dissociate into CH with an activation barrier of only 26.1 kJ mol^{-1}, while CH hydrogenation to CH_2 has a relatively high activation barrier of 71.6 kJ mol^{-1}. This result suggests that CH_2 should be the least stable species among all the dissociation products. Hence, the lifetime of CH_2 is likely short, and its concentration is rather low on the surface. Moreover, the high activation barrier of CH dissociation to C + H indicates that this elementary reaction is unfavourable in CH_4 dissociation. Therefore, among all dissociated CH_x (x = 0–3) species from methane, CH should be the most abundant species on the Rh(111) surface, in agreement with previous studies.[31,45]

3.3. CH_x (x = 1–3) formation from syngas

For CH_x (x = 1–3) formation from syngas, there are two possibilities: one is the direct dissociation of CO to produce C + O followed by the hydrogenation of C to form CH_x species; the other is the hydrogenation of CO to CH_xO or CH_xOH species followed by the direct dissociation or H-assisted dissociation to CH_x species. In the following section, the above two possibilities for CH_x (x = 1–3) formation are investigated.

3.3.1. Initial CO step. Three possible reactions exist for the initial CO step: direct CO dissociation; CO hydrogenation to CHO; and CO hydrogenation to COH. The corresponding potential energy profiles together with the structures of initial

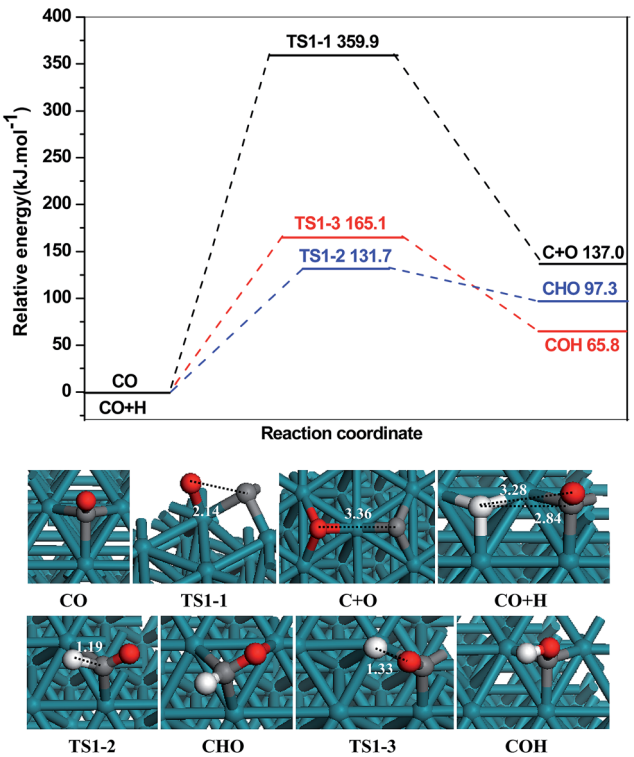

Fig. 4 The potential energy profile of the initial CO step together with the structures of initial states, transition states and final states. Bond lengths are in Å.

states, transition states and final states are displayed in Fig. 2 and 4.

$CO \rightarrow C + O$ R1-1
$CO + H \rightarrow CHO$ R1-2
$CO + H \rightarrow COH$ R1-3

For direct CO dissociation in R1-1, starting from adsorbed CO, CO dissociates into C + O *via* a transition state TS1-1. The distance between C and O atoms is elongated to 2.14 Å in TS1-1 and 3.36 Å in C + O. This dissociation process is endothermic by 137.0 kJ mol^{-1} with a relatively high activation barrier of 359.9 kJ mol^{-1}.

For CHO formation in R1-2, starting from CO + H, CO adsorbs at the hcp site, and H adsorbs at the adjacent hcp site. The H adatom moves toward the C atom of CO *via* the transition state TS1-2 to produce CHO; the distance between H and C atoms is decreased to 1.19 Å in TS1-2 from 2.84 Å in CO + H; this elementary reaction is endothermic by 97.3 kJ mol^{-1} and has an activation barrier of 131.7 kJ mol^{-1}. As for COH formation in R1-3, H adatom approaches the O atom of CO through the transition state TS1-3, in which the distance between H and O atoms is decreased to 1.33 Å from 3.28 Å in CO + H; the activation barrier of this elementary reaction is 165.1 kJ mol^{-1}, and the reaction is endothermic by 65.8 kJ mol^{-1}. A previous study by Choi and Liu[16] showed that the activation barriers of the above three elementary reactions (R1-1, R1-2 and R1-3) on the Rh(111) surface are 3.72, 1.35 and 1.67 eV, respectively, which are all close to our results.

The above results show that while CO and H are co-adsorbed on the Rh(111) surface, the catalytic activity for direct CO dissociation is rather low, which agrees well with a previous study by Mavrikakis *et al.*[46] CO hydrogenation to CHO or COH is more favourable than direct CO dissociation, and CHO formation is more preferred. Namely, CHO is the major product of the initial CO step, and the subsequent reactions including the formation of CH_x, CH_xO and CH_xOH only start with CHO.

3.3.2. CH formation. Starting from CHO, CH can be produced by CHO and CHOH. First, CHO hydrogenation to CHOH is considered (R2-1), and the direct dissociation and H-assisted dissociation of CHO and CHOH to form CH are subsequently discussed (R2-2–R2-5). The potential energy profiles of these reactions together with the corresponding structures are shown in Fig. 2 and 5.

$CHO + H \rightarrow CHOH$ R2-1
$CHO \rightarrow CH + O$ R2-2
$CHOH \rightarrow CH + OH$ R2-3
$CHO + H \rightarrow CH + OH$ R2-4
$CHOH + H \rightarrow CH + H_2O$ R2-5

For R2-1, starting from CHO + H, H adatom is transferred to the adsorbed CHO to form CHOH through a transition state TS2-1. The distance between H adatom and O atoms is decreased to 1.56 Å in TS2-1 from 2.71 Å in CHO + H; this elementary reaction is endothermic by 30.9 kJ mol^{-1} with an activation barrier of 105.1 kJ mol^{-1}.

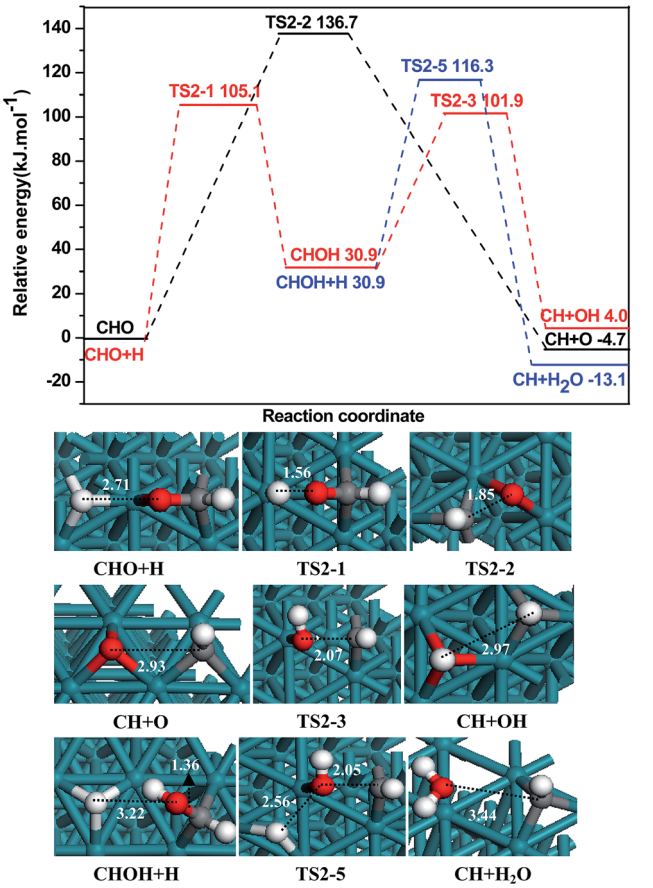

Fig. 5 The potential energy profile of CH formation together with the structures of initial states, transition states and final states. Bond lengths are in Å.

For non-H-assisted CH formation, in R2-2, the C–O bond cleavage of CHO proceeds through the transition state TS2-2 to produce CH + O. The distance between C and O atoms is elongated from 1.30 Å in CHO to 1.85 Å in TS2-2 and 2.93 Å in CH + O. The activation barrier of this elementary reaction is 136.7 kJ mol^{-1}, and the reaction is slightly exothermic by 4.7 kJ mol^{-1}. In R2-3, the C–O bond cleavage of CHOH can lead to CH + OH *via* the transition state TS2-3. The C–O bond distance undergoes an elongation from 1.36 Å in CHOH to 2.07 Å in TS2-3 and 2.97 Å in CH + OH. This elementary reaction is exothermic by 26.9 kJ mol^{-1} with an activation barrier of 71.0 kJ mol^{-1}.

For H-assisted CH formation, in R2-4, the obtained TS for the C–O bond scission of CHO assisted by H is similar to that of CHOH dissociation to CH + OH; this indicates that the first step of H-assisted CHO dissociation is hydrogenation to CHOH rather than the formation of CH + OH. In R2-5, beginning with the initial state, CHOH + H and CHOH adsorb at the bridge site, and H locates at the hcp site. Assisted by H, CHOH then dissociates into CH + H_2O *via* the transition state TS2-5. In the final state, CH + H_2O, CH adsorbs at the fcc site, while H_2O is far away from the surface with its molecular plane nearly parallel to the surface. The distance between C and O atoms is elongated to 2.05 Å in TS2-5 and 3.44 Å in CH + H_2O; meanwhile, the distance between H adatom and O atoms is decreased to 2.56 Å in TS2-5

from 3.22 Å in CHOH + H. The activation barrier of this elementary step is 85.4 kJ mol^{-1}, and the reaction is exothermic by 44.0 kJ mol^{-1}.

Fig. 5 shows that among the three possible CH formation reactions, CH is dominantly formed by the direct C–O bond scission of the CHOH intermediate (red line), which has the highest barrier of 105.1 kJ mol^{-1}. The rate-controlling step of this route occurs at TS2-1 with an activation barrier and reaction energy of 105.1 and 30.9 kJ mol^{-1}, respectively.

3.3.3. CH_2 and CH_3 formation. There are two possibilities for CH_2 and CH_3 formation: the direct dissociation of CH_xO or CH_xOH; and the H-assisted dissociation of $CH_{x-1}O$, $CH_{x-1}OH$, CH_xO and CH_xOH, where $x = 2$ and 3 correspond to CH_2 and CH_3 formation, respectively. The potential energy profiles of CH_2 and CH_3 formation together with the corresponding structures are displayed in Fig. 2, 6 and 7.

$CHO + H \rightarrow CH_2O$	R3-1	$CH_2O + H \rightarrow CH_3O$	R4-1
$CH_2O + H \rightarrow CH_2OH$	R3-2	$CH_3O + H \rightarrow CH_3OH$	R4-2
$CHOH + H \rightarrow CH_2OH$	R3-3	$CH_2OH + H \rightarrow CH_3OH$	R4-3
$CH_2O \rightarrow CH_2 + O$	R3-4	$CH_3O \rightarrow CH_3 + O$	R4-4
$CH_2OH \rightarrow CH_2 + OH$	R3-5	$CH_3OH \rightarrow CH_3 + OH$	R4-5
$CHO + H \rightarrow CH_2 + O$	R3-6	$CH_2O + H \rightarrow CH_3 + O$	R4-6
$CH_2O + H \rightarrow CH_2 + OH$	R3-7	$CH_3O + H \rightarrow CH_3 + OH$	R4-7
$CHOH + H \rightarrow CH_2 + OH$	R3-8	$CH_2OH + H \rightarrow CH_3 + OH$	R4-8
$CH_2OH + H \rightarrow CH_2 + H_2O$	R3-9	$CH_3OH + H \rightarrow CH_3 + H_2O$	R4-9

CH_2 formation. The C_1 oxygenate formation related to CH_2 formation is first investigated. In R3-1, beginning with CHO + H, H adatom approaches the C atom of CHO to form CH_2O *via* the transition state TS3-1. In TS3-1, the distance between H and C atoms is decreased to 1.25 Å from 2.88 Å in CHO + H. This elementary reaction is endothermic by 49.3 kJ mol^{-1} with an activation barrier of 68.8 kJ mol^{-1}. In R3-2, starting from CH_2O + H, the co-adsorbed CH_2O and H go through the transition state TS3-2 to form CH_2OH; the distance between H and O atoms is decreased to 1.51 Å in TS3-2 from 3.00 Å in CH_2O + H. This elementary reaction is endothermic by 3.1 kJ mol^{-1} with an activation barrier of 79.3 kJ mol^{-1}. In R3-3, the adsorbed H adatom is transferred to CHOH to form CH_2OH *via* the transition state TS3-3; the distance between H adatom and C atoms is decreased to 1.48 Å in TS3-3 from 2.98 Å in CHOH + H. The activation barrier of this elementary reaction is 64.2 kJ mol^{-1}, and it is endothermic by 21.5 kJ mol^{-1}.

For CH_2 formation without H assistance, in R3-4, CH_2O directly dissociates into CH_2 + O *via* the transition state TS3-4; the distance between C and O atoms is extended to 2.05 Å in TS3-4 and 3.26 Å in CH_2 + O from 1.39 Å in CH_2O. The activation barrier of this elementary reaction is 109.5 kJ mol^{-1}, and the reaction is exothermic by 5.6 kJ mol^{-1}. In R3-5, the C–O bond cleavage of CH_2OH can produce CH_2 + OH *via* the transition state TS3-5; the distance between C and O atoms is elongated to 2.98 Å in TS3-5 and 3.03 Å in CH_2 + OH from 1.46 Å in CH_2OH. This elementary reaction is endothermic by 25.9 kJ mol^{-1} with an activation barrier of 106.5 kJ mol^{-1}.

For H-assisted CH_2 formation, in R3-6, the TS obtained for the H-assisted C–O bond scission of CHO to form CH_2 + O is similar to the TS of direct CH_2O dissociation; this suggests that the H-assisted dissociation of CHO first produces CH_2O rather than being dissociated into CH_2 + O. In R3-7, CH_2O dissociates into CH_2 + OH with H assistance. The TS obtained for this reaction is similar to that formed during CH_2O hydrogenation to CH_2OH, indicating that CH_2O prefers to be hydrogenated to CH_2OH rather than being dissociated into CH_2 + OH. In R3-8, the TS obtained for H-assisted C–O bond cleavage of CHOH to produce CH_2 + OH is similar to the TS for CH_2OH dissociation, indicating that CHOH with H assistance prefers to be hydrogenated to CH_2OH rather than dissociated to CH_2 + OH. In R3-9, H-assisted CH_2OH goes through the transition state TS3-9 to form CH_2 + H_2O. The distance between C and O atoms is elongated to 2.70 Å in TS3-9 and 3.44 Å in CH_2 + H_2O from 1.44 Å in CH_2OH + H; meanwhile, the distance between H and O atoms is shortened from 2.61 Å in CH_2OH + H to 1.60 Å in TS3-9. In the final state, CH_2 + H_2O, CH_2 adsorbs at the fcc site, and H_2O is far from the surface with its molecular plane nearly parallel to the surface. This elementary reaction has an activation barrier of 148.5 kJ mol^{-1} and is exothermic by 28.7 kJ mol^{-1}.

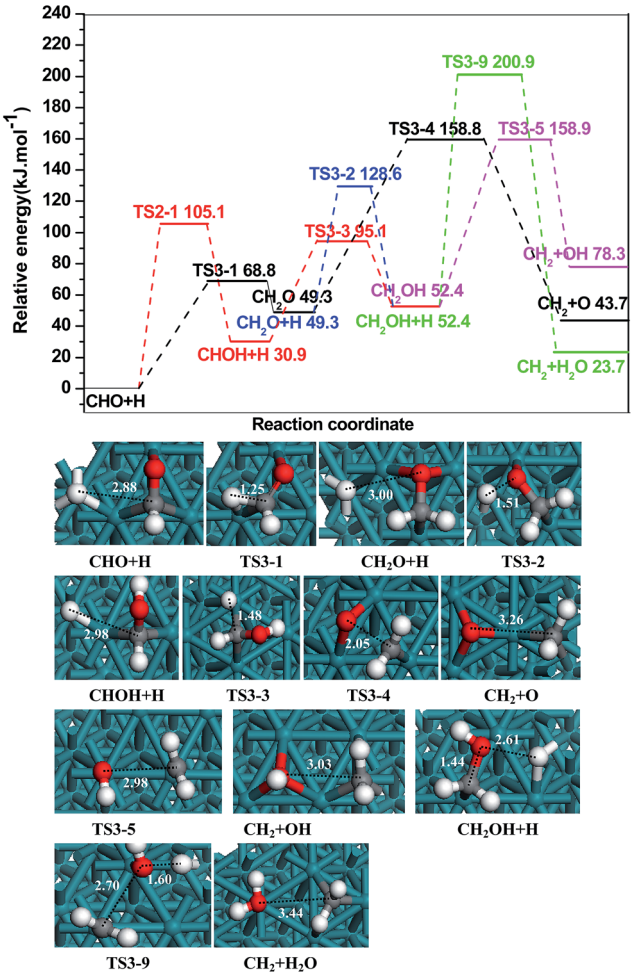

Fig. 6 The potential energy profile of CH_2 formation together with the structures of initial states, transition states and final states. Bond lengths are in Å.

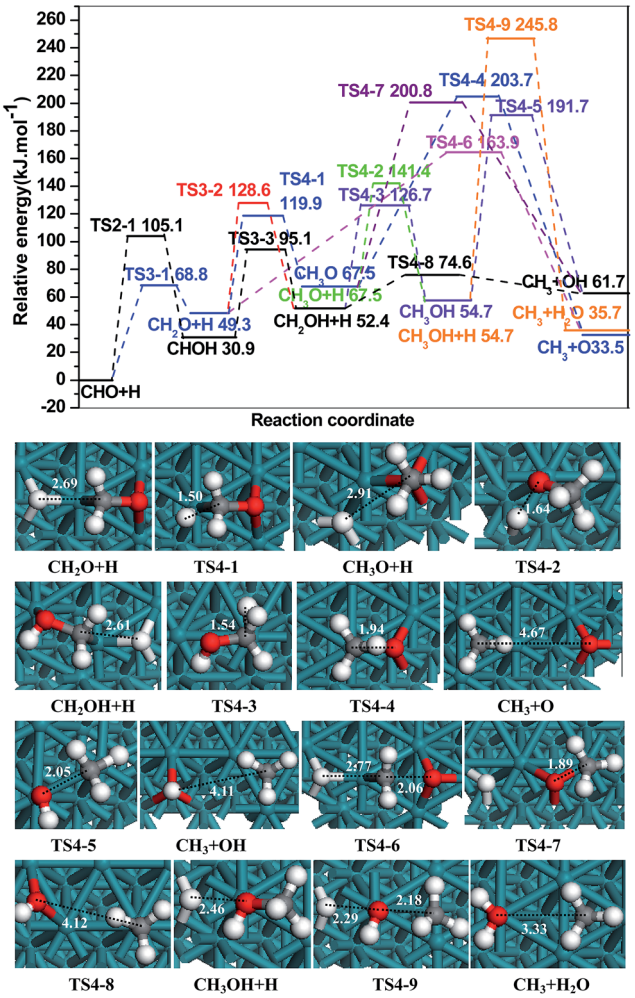

Fig. 7 The potential energy profile of CH_3 formation together with the structures of initial states, transition states and final states. Bond lengths are in Å.

Fig. 6 shows that with respect to the initial state CHO + H, three parallel routes (CHO + H → CH_2O → CH_2 + O, CHO + 2H → CHOH + H → CH_2OH → CH_2 + OH and CHO + 2H → CH_2O + H → CH_2OH → CH_2 + OH) are responsible for CH_2 formation. The corresponding highest barriers are 158.8, 158.9 and 158.9 kJ mol^{-1}, respectively, and the rate-controlling steps of these three routes occur at TS3-4, TS3-5 and TS3-5 with the activation barriers of 109.5, 106.5 and 106.5 kJ mol^{-1}, respectively.

CH_3 formation. Similar to CH_2 formation, the C_1 oxygenate formation related to CH_3 formation is first investigated (R4-1–R4-3), in which H adatom approaches the C atom of CH_2O to produce CH_3O *via* the transition state TS4-1. CH_3O is hydrogenated to form CH_3OH *via* the transition state TS4-2, and CH_2OH is hydrogenated to form CH_3OH *via* the transition state TS4-3. The activation barriers for these three reactions are 70.6, 73.9 and 74.3 kJ mol^{-1} with corresponding reaction energies of 18.2, −12.8 and 2.3 kJ mol^{-1}, respectively.

R4-4 and R4-5 are the direct dissociations of CH_3O and CH_3OH to form CH_3 species *via* the transition states TS4-4 and TS4-5, respectively; these transition states have corresponding activation barriers of 136.2 and 137.0 kJ mol^{-1} with reaction energies of −34.0 and 7.0 kJ mol^{-1}, respectively. In R4-6, CH_2O undergoes H-assisted dissociation into CH_3 + O *via* the transition state TS4-6. The distance between C and O atoms, which is 1.39 Å in CH_2O + H, is elongated to 2.06 Å in TS4-6 and 4.67 Å in CH_3 + O, while the distance between H and C atoms is shortened from 2.69 Å in CH_2O + H to 1.12 Å in CH_3 + O. This elementary reaction is exothermic by 15.8 kJ mol^{-1} with an activation barrier of 114.6 kJ mol^{-1}. In R4-7, the H-assisted C–O bond cleavage of CH_3O can form CH_3 + OH *via* the transition state TS4-7. The distance between C and O atoms is 1.43 Å in CH_3O + H, and it is extended to 1.89 Å in TS4-7 and 4.11 Å in CH_3 + OH. The activation barrier of this elementary reaction is 133.3 kJ mol^{-1}, and it is slightly exothermic by 5.8 kJ mol^{-1}. In R4-8, CH_2OH with H assistance can break the C–O bond *via* the transition state TS4-8 to form CH_3 + OH. The distance between C and O atoms is elongated to 4.12 Å in TS4-8 from 1.45 Å in CH_2OH + H. This elementary reaction is endothermic by 9.3 kJ mol^{-1} with an activation barrier of only 22.2 kJ mol^{-1}. In R4-9, the H-assisted C–O bond cleavage of CH_3OH can form CH_3 + H_2O *via* the transition state TS4-9. The distance between H adatom and O atoms is shortened to 2.29 Å in TS4-9 from 2.46 Å in CH_3OH + H; meanwhile, the distance between C and O atoms is extended from 1.45 Å in CH_3OH + H to 2.18 Å in TS4-9 and 3.33 Å in CH_3 + H_2O. In CH_3 + H_2O, CH_3 adsorbs at the fcc site, while H_2O locates at the top site with its molecular plane nearly parallel to the surface. The activation barrier of this elementary reaction is 191.1 kJ mol^{-1}, and it is exothermic by 19.0 kJ mol^{-1}.

Fig. 7 shows that with respect to the initial state CHO + H, the route of CHO + H → CHOH + H → CH_2OH + H → CH_3 + OH is the most kinetically favourable (black line). The highest barrier of this route is 105.1 kJ mol^{-1}, and the rate-controlling step occurs at TS2-1 with an activation barrier of 105.1 kJ mol^{-1}.

3.3.4. CH_3OH formation. Previous studies[47,48] have suggested that Rh metallic catalysts can also convert syngas to methanol *via* CH_xO and CH_xOH hydrogenation. In this section, we further investigate the mechanism of CH_3OH formation from syngas to probe the effect of CH_3OH formation on CH_x formation. Fig. 8 presents a summary potential energy profiles for three possible routes of CH_3OH formation with respect to CHO + H.

We can see that the routes CHO + H → CHOH + H → CH_2OH + H → CH_3OH, CHO + H → CH_2O + H → CH_2OH + H → CH_3OH and CHO + H → CH_2O + H → CH_3O + H → CH_3OH have the highest barriers of 126.7, 128.6 and 141.4 kJ mol^{-1}, respectively. As a result, the former two routes are responsible for CH_3OH formation from syngas, and the rate-controlling steps occur at TS4-3 and TS3-2 with corresponding activation barriers of 74.3 and 79.3 kJ mol^{-1}, respectively.

3.3.5. Brief summary. The above results show that CO hydrogenation is much more favourable than CO dissociation, and CO hydrogenation to CHO is more favourable than CO hydrogenation to COH. Thus, all CH_x (x = 1–3) formation starts from CHO or CHO + H. Meanwhile, with respect to CHO + H, we obtain the highest barrier for the optimal paths of CH_x (x = 1–3) species and CH_3OH formation; the results show that CH

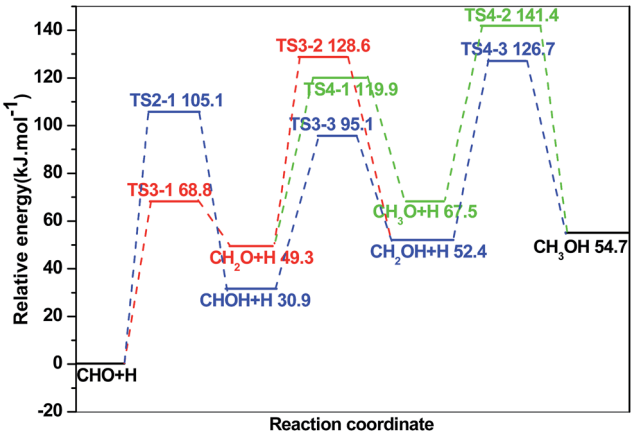

Fig. 8 The potential energy profile of CH_3OH formation.

formation has the highest barrier of 105.1 kJ mol^{-1}. For CH_2 formation, three parallel routes have the highest barriers of 158.8, 158.9 and 158.9 kJ mol^{-1}, and CH_3 formation has the highest barrier of 105.1 kJ mol^{-1}. For CH_3OH formation, two parallel routes have the highest barriers of 128.6 and 126.7 kJ mol^{-1}, respectively.

On the basis of the barriers for these reactions toward CH_x ($x = 1$–3) and CH_3OH formation, we can conclude that CH and CH_3 formation have the same highest barriers; both are more favourable than CH_2 and CH_3OH formation, suggesting that CH and CH_3 are the most abundant syngas-derived CH_x species on the Rh(111) surface.

3.4. General discussion

On the basis of the above results, we can determine the major form of CH_x ($x = 1$–3) produced from methane and syngas. For methane, CH formed by the successive dehydrogenation of CH_4 is the most abundant species; for syngas, CH and CH_3 produced by the two routes CO + 2H → CHO + H → CHOH → CH + OH and CO + 4H → CHO + 3H → CHOH + 2H → CH_2OH + H → CH_3 + OH are the most abundant species.

Compared to previous studies, the reaction routes considered in our study are more detailed; for example, for the formation mechanism of CH_x ($x = 1$–3) species, Kapur *et al.*[15] did not consider CH_2 and CH_3 formation from the direct dissociation of CH_2OH and CH_3OH, respectively, or the H-assisted formation routes of CH_x ($x = 1$–3) species. Choi and Liu[16] only considered CH_3 formation *via* the direct dissociation of CH_3O, while CH_3 formation *via* H-assisted routes along with the formation mechanisms of CH and CH_2 were not discussed. In our study, the H-assisted routes of CH_x ($x = 1$–3) formation are systematically investigated; for example, for CH formation, the H-assisted routes of CHO + H → CH + OH and CHOH + H → CH + H_2O are discussed. Similarly, for CH_2 formation, the H-assisted routes of CH_2O + H → CH_2 + OH, CHOH + H → CH_2 + OH and CH_2OH + H → CH_2 + H_2O are discussed, and the H-assisted routes of CH_2O + H → CH_3 + O, CH_3O + H → CH_3 + OH, CH_2OH + H → CH_3 + OH and CH_3OH + H → CH_3 + H_2O are discussed for CH_3 formation. Meanwhile, the direct dissociation of CH_2OH to form CH_2 species as well as the direct dissociation of CH_3OH to CH_3 species are also considered. As a result, the most favourable routes of CH_x formation obtained in our study are different from those obtained by previous studies. For example, previous studies[15,16] have suggested that the most favourable route for CH_3 formation is CO + 3H → CHO + 2H → CH_2O + H → CH_3O → CH_3 + O; however, in our study, the most favourable route of CH_3 formation is CO + 4H → CHO + 3H → CHOH + 2H → CH_2OH + H → CH_3 + OH.

Fig. 9 presents the highest barrier profiles for the most favourable formation routes of CH_x ($x = 1$–3) species and CO insertion into CH_x ($x = 1$–3) species involved in acetic acid synthesis from methane–syngas. We can see that the highest barrier of CH formation from CH_4 is 73.6 kJ mol^{-1}, while CH and CH_3 formation from syngas have the same highest barrier of 202.4 kJ mol^{-1}. Taking reaction energy into consideration, it is found that CH species from CH_4 are more favourable both kinetically and thermodynamically compared to CH and CH_3 formation from syngas. As a result, CH species obtained by CH_4 dissociation should be the main source and predominant form of CH_x ($x = 1$–3); these species can boost the kinetics of acetic acid synthesis from methane–syngas, and CO insertion into CH_x ($x = 1$–3) species should be responsible for the formation of C_2 oxygenate acetic acid precursors.

To confirm the above results, CO insertion into CH_x ($x = 1$–3) species has been examined, suggesting that CO insertion into CH to form CHCO is endothermic by 91.1 kJ mol^{-1} with an activation barrier of 120.6 kJ mol^{-1}. CH_2CO formation by CO insertion into CH_2 has an activation barrier of 113.5 kJ mol^{-1}, and this reaction is endothermic by 72.0 kJ mol^{-1}. CH_3CO formation by CO insertion into CH_3 is endothermic by 19.9 kJ mol^{-1} and has an activation barrier of 143.0 kJ mol^{-1}. It can be found that the reaction barrier of 143.0 kJ mol^{-1} obtained in our study is much higher than that reported in previous studies;[15,16] this can be attributed to the different slab models employed for the calculation. In the previous studies by Kapur *et al.*[15] and Choi and Liu,[16] the slab model employed was a three-layer $p(2 \times 2)$ supercell, and the calculated reaction

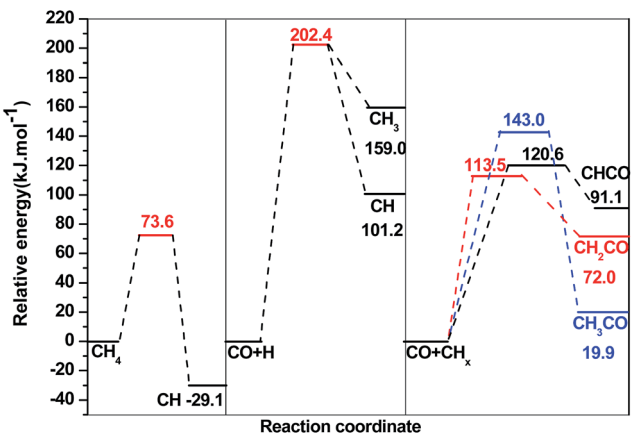

Fig. 9 The highest barrier profiles for the formation of the most favourable products: CH *via* methane; CH and CH_3 *via* syngas; and CO insertion into CH_x.

barriers are 126.4 and 111.0 kJ mol^{-1}, respectively; however, Zhao *et al.*[17] used a four-layer $p(3 \times 3)$ model for the Rh catalyst, and a higher reaction barrier of 149.6 kJ mol^{-1} was obtained. In this study, a four-layer $p(3 \times 3)$ slab model is employed, and the calculated results show that the reaction barrier is 143.0 kJ mol^{-1}, close to that obtained by Zhao *et al.*[17] using the same slab model. The differences in calculation parameters might also lead to the different calculation results. For example, in a previous study by Choi and Liu,[16] spin-polarisation calculations were carried out throughout all calculations, and the transition states were obtained with the CI-NEB method; conversely, in our study, the spin-polarisation calculations are only considered for isolated atoms and molecules since we have confirmed that spin-polarisation does not have a significant effect on the energetics of calculations for the periodic slab model. In addition, the transition states obtained with the CI-NEB method are optimised using the dimer method. Although the calculated results of specific reactions in our study are different from those of previous studies, the qualitative conclusions in our study are in accordance with those obtained by the previous studies;[15,17] for example, for CO insertion into CH_x (x = 1–3) species, CO insertion into CH_3 has the highest reaction barrier among the three reactions, and the reaction barrier for CO insertion into CH is higher than that for CO insertion into CH_2. On the other hand, in contrast to previous studies where CO insertion into CH_x (x = 1–3) was calculated to identify the optimal routes for C_2 oxygenate formation, CO insertion into CH_x (x = 1–3) in our study is performed for comparison with CO hydrogenation, in which the role of CO in acetic acid synthesis is clarified. On the basis of the above discussion, we can find that CO insertion into CH_x species is more favourable than CO hydrogenation to form CH and CH_3 species; namely, CO predominantly inserts into CH_x rather than being hydrogenated during the synthesis of acetic acid from methane–syngas on Rh(111).

To further understand the effect of reaction temperature on the kinetics of CH_x formation on the Rh(111) surface, we have further calculated the rate constants of three key steps at different temperatures; the selected three key steps are CH_4 dehydrogenation to CH_3, CO hydrogenation to CHO and CO insertion into CH. Previous studies have reported that Rh-based catalysts exhibit a good catalytic activity toward C_2 oxygenates when the reaction temperature ranges from 563 K to 593 K.[5,49,50] Hence, on the basis of the Eyring's transition state theory (TST),[51] the rate constants of these three key steps at T = 550, 575 and 600 K have been calculated, and the corresponding results are listed in Table 1. A detailed description of the rate constant calculation is given in the ESI.†

Table 1 Rate constant k for the key elementary reactions involved in acetic acid synthesis on the Rh(111) surface at different temperatures

	Rate constant k/s^{-1}		
Elementary reactions	550 K	575 K	600 K
$CH_4 \rightarrow CH_3 + H$	1.52×10^5	2.87×10^5	5.14×10^5
$CO + H \rightarrow CHO$	6.55×10^{-3}	2.49×10^{-2}	8.52×10^{-2}
$CH + CO \rightarrow CHCO$	3.37	11.08	32.98

Table 1 shows that the rate constant k of these reactions all increase with increasing temperature on the Rh(111) surface. At the same temperature, the rate constants of CH_4 dehydrogenation and CO insertion into CH are much larger than that of CO hydrogenation; namely, both CH_4 dehydrogenation and CO insertion reactions occur much more easily than CO hydrogenation on the Rh(111) surface. Thus, in the synthesis of acetic acid from methane–syngas, CH_x intermediates obtained from methane are more favourable, and CO mainly participates in insertion reactions rather than in its hydrogenation.

Therefore, in the synthesis of acetic acid from methane–syngas on the Rh(111) surface, the primary CH_x (x = 1–3) species is CH, which comes primarily from CH_4 dehydrogenation rather than from syngas; the CO in syngas mainly participates in insertion reactions to form CHCO as a C_2 oxygenate precursor of acetic acid.

3.5. The formation of acetic acid

The above results suggest that CH and CO will be the main intermediates on the Rh(111) surface for further reactions to form the C–C chain in the methane–syngas conversion to acetic acid. Thus, the CHCO intermediate is considered as the initial C_2 precursor of acetic acid. As a result, starting from CHCO, we further investigate the formation of acetic acid.

$CHCO + OH \rightarrow CHCOOH$	R5-1
$CHCO + H \rightarrow CH_2CO$	R5-2
$CH_2CO + OH \rightarrow CH_2COOH$	R5-3
$CH_2CO + H \rightarrow CH_3CO$	R5-4
$CH_3CO + OH \rightarrow CH_3COOH$	R5-5
$CHCOOH + H \rightarrow CH_2COOH$	R5-6
$CH_2COOH + H \rightarrow CH_3COOH$	R5-7

Our results show that the activation barrier of the reaction of CHCO with OH to form CHCOOH in R5-1 is 65.5 kJ mol^{-1}, and this reaction is exothermic by 56.8 kJ mol^{-1}. In R5-2, CHCO hydrogenation to CH_2CO has an activation barrier of 63.0 kJ mol^{-1}, and this reaction is endothermic by 24.7 kJ mol^{-1}. In R5-3, the formation of CH_2COOH from CH_2CO + OH is exothermic by 39.6 kJ mol^{-1} with an activation barrier of 60.6 kJ mol^{-1}. For R5-4, CH_2CO hydrogenation to CH_3CO is exothermic by 46.2 kJ mol^{-1} and has an activation barrier of 63.2 kJ mol^{-1}. The formation of CH_3COOH from CH_3CO + OH in R5-5 is exothermic by 26.2 kJ mol^{-1} with an activation barrier of 54.3 kJ mol^{-1}. On the other hand, the hydrogenation of CHCOOH and CH_2COOH in R5-6 and R5-7 have activation barriers of 66.8 and 51.1 kJ mol^{-1}, respectively; CHCOOH hydrogenation is endothermic by 21.8 kJ mol^{-1}, while CH_2COOH hydrogenation is exothermic by 19.9 kJ mol^{-1}.

Therefore, based on the energy barriers of each route, we find that acetic acid formation through the pathway CHCO → CHCOOH → CH_2COOH → CH_3COOH is most favourable. Interestingly, previous studies[52,53] have reported that CH, CO and CHCO are the possible intermediates involved in the formation of C_2 oxygenates; our results are consistent with their conclusions.

3.6. Microkinetic modelling

In order to estimate the formation rates of the major products involved in the synthesis of acetic acid from methane–syngas, a microkinetic model[54,55] has been employed in our study. On the basis of the calculated results for acetic acid synthesis from methane–syngas on the Rh(111) surface, the major products are expected to be CH_3COOH and CH_3OH. Thus, the rates for CH_3COOH and CH_3OH production and the selectivity of CH_3COOH are estimated under the typical synthetic conditions. All the elementary reaction steps involved in the optimal reaction routes together with the corresponding activation barriers are listed in Table 2. The adsorption processes of methane, water and syngas are assumed to be in equilibrium in our study. Meanwhile, the pseudo-steady-state approximation[55] is applied for other minority species on the catalyst surface; that is, the production rates and consumption rates for all species involved are considered to be the same. A detailed description of the microkinetic model is given in the ESI.†

Table 2 Elementary reactions involved in the optimal routes for CH_3COOH and CH_3OH synthesis and the corresponding reaction barriers for the microkinetic model

Elementary reactions		E_a/kJ mol^{-1}
R1	$CH_4 \rightarrow CH_3 + H$	73.6
R2	$CH_3 \rightarrow CH_2 + H$	46.9
R3	$CH_2 \rightarrow CH + H$	26.1
R4	$CH + CO \rightarrow CHCO$	120.6
R5	$CHCO + OH \rightarrow CHCOOH$	65.5
R6	$CHCOOH + H \rightarrow CH_2COOH$	66.8
R7	$CH_2COOH + H \rightarrow CH_3COOH$	51.1
R8	$H_2O \rightarrow OH + H$	92.2
R9	$CO + H \rightarrow CHO$	131.7
R10	$CHO + H \rightarrow CHOH$	105.1
R11	$CHOH + H \rightarrow CH_2OH$	64.2
R12	$CH_2OH + H \rightarrow CH_3OH$	74.3
R13	$CHO + H \rightarrow CH_2O$	68.8
R14	$CH_2O + H \rightarrow CH_2OH$	79.3

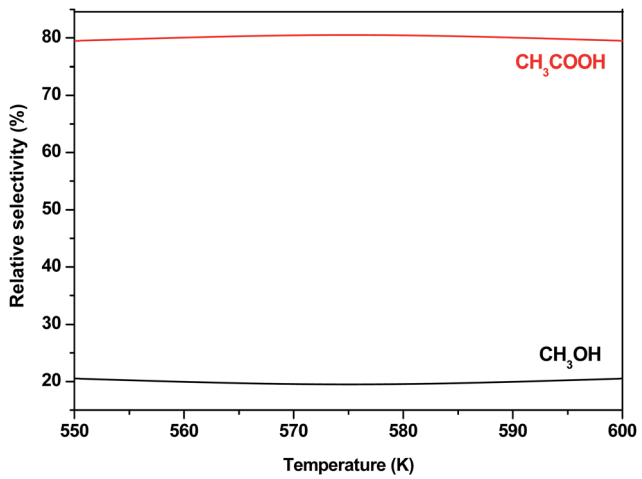

Fig. 10 The relative selectivity of major products (acetic acid and methanol) from methane–syngas on the Rh(111) surface at different temperatures from microkinetic modelling.

According to the microkinetic model and the calculated energies in our study, the reaction rates and the relative selectivity of CH_3COOH (r_{CH_3COOH}) and CH_3OH (r_{CH_3OH}) production are estimated under typical experimental conditions ($P_{CH_4} = 4$ atm, $P_{H_2O} = 4$ atm, $P_{CO} = 4$ atm, $P_{H_2} = 8$ atm, $T = 550$–600 K). The calculated relative selectivities of CH_3COOH and CH_3OH are displayed in Fig. 10; these suggest that the major product during the synthesis of acetic acid from methane–syngas on the Rh(111) surface is CH_3COOH, and that the production of CH_3OH can not compete with that of CH_3COOH. Meanwhile, the highest relative selectivity for CH_3COOH is obtained at 575 K, in accordance with previous experimental results demonstrating that Rh-based catalysts exhibit good catalytic activities toward C_2 oxygenates at reaction temperatures ranging from 563 K to 593 K.[5,49,50]

4. Conclusions

In this study, the formation mechanisms of CH_x (x = 1–3) species involved in acetic acid synthesis from methane–syngas on the Rh(111) surface have been systematically investigated using DFT calculations. Our results show that CH is the dominant product of methane dissociation, while for CH_x (x = 1–3) formation from syngas, CO hydrogenation is favoured compared to CO dissociation, and CO hydrogenation to CHO is preferred over COH formation. Starting from CHO, CH and CH_3 species are the dominant products rather than CH_2 and CH_3OH on the Rh(111) surface. On the other hand, CH species from CH_4 are favourable both kinetically and thermodynamically compared to CH and CH_3 formation from syngas; meanwhile, CO insertion into CH_x (x = 1–3) species occurs preferentially over CO hydrogenation. As a result, for acetic acid synthesis from methane–syngas on the Rh(111) surface, the major CH_x (x = 1–3) species is CH, which is derived from methane; CO in syngas mainly participates in insertion reactions to produce CHCO, which is the C_2 oxygenate precursor leading to the formation of acetic acid *via* the route $CHCO \rightarrow CHCOOH \rightarrow CH_2COOH \rightarrow CH_3COOH$. Furthermore, microkinetic modelling analysis shows that the major product of acetic acid synthesis from methane–syngas on the Rh(111) surface is CH_3COOH, and that the production of CH_3OH can not compete with that of CH_3COOH.

Acknowledgements

This work is financially supported by the National Natural Science Foundation of China (no. 21276003, 21476155 and 21276171), the Natural Science Foundation of Shanxi Province (no. 2014011012-2) and the Top Young Innovative Talents of Shanxi.

References

1 N. Yoneda, S. Kusano, M. Yasui, P. Pujado and S. Wilcher, Recent Advances in Processes and Catalysts for the

Production of Acetic Acid, *Appl. Catal. A: Gen.*, 2001, **221**, 253–265.
2 Y. Ben, C. Liu and K. Yu, Study of C_1-chemical Products in the Acetic Acid Synthesis, *Chem. Ind. Eng.*, 2004, **21**, 96–100.
3 J. H. Lunsford, Catalytic Conversion of Methane to More Useful Chemicals and Fuels: A Challenge for the 21st Century, *Catal. Today*, 2000, **63**, 165–174.
4 A. Sen, Catalytic Functionalization of Carbon–Hydrogen and Carbon–Carbon Bonds in Protic Media, *Acc. Chem. Res.*, 1998, **31**, 550–557.
5 P. Z. Lin, D. B. Liang, H. Y. Luo, C. H. Xu, H. W. Zhou, S. Y. Huang and L. W. Lin, Synthesis of C_{2+}-oxygenated Compounds Directly From Syngas, *Appl. Catal. A: Gen.*, 1995, **131**, 207–214.
6 K. X. Wang, H. F. Xu, W. S. Li and X. P. Zhou, Acetic acid synthesis from methane by non-synthesis gas process, *J. Mol. Catal. A: Chem.*, 2005, **225**, 65–69.
7 K. X. Wang, H. F. Xu, W. S. Li, C. T. Au and X. P. Zhou, The Synthesis of Acetic Acid From Methane *via* Oxidative Bromination, Carbonylation, and Hydrolysis, *Appl. Catal. A: Gen.*, 2006, **304**, 168–177.
8 B. Q. Xu and W. M. H. Sachtler, Rh/NaY: A Selective Catalyst for Direct Synthesis of Acetic Acid from Syngas, *J. Catal.*, 1998, **180**, 194–206.
9 B. Q. Xu, K. Q. Sun, Q. M. Zhu and W. M. H. Sachtler, Unusual Selectivity of Oxygenate Synthesis Formation of Acetic Acid From Syngas over Unpromoted Rh in NaY Zeolite, *Catal. Today*, 2000, **63**, 453–460.
10 Y. Taniguchi, T. Hayashida, H. Shibasaki, D. Piao, T. Kitamura, T. Yamaji and Y. Fujiwara, Highly Efficient Vanadium-Catalyzed Transformation of CH_4 and CO to Acetic Acid, *Org. Lett.*, 1999, **1**, 557–559.
11 M. Asadullah, T. Kitamura and Y. Fujiwara, Calcium-Catalyzed Selective and Quantitative Transformation of CH_4 and CO into Acetic Acid, *Angew. Chem., Int. Ed.*, 2000, **39**, 2475–2478.
12 S. J. Chempath and A. T. Bell, Density Functional Theory Analysis of the Reaction Pathway for Methane Oxidation to Acetic Acid Catalyzed by Pd^{2+} in Sulfuric Acid, *J. Am. Chem. Soc.*, 2006, **128**, 4650–4657.
13 M. V. Kirillova, M. L. Kuznetsov, P. M. Reis, J. A. L. da Silva, J. J. R. F. da Silva and A. J. L. Pombeiro, Direct and Remarkably Efficient Conversion of Methane into Acetic Acid Catalyzed by Amavadine and Related Vanadium Complexes. A Synthetic and a Theoretical DFT Mechanistic Study, *J. Am. Chem. Soc.*, 2007, **129**, 10531–10545.
14 I. H. Hristov and T. Ziegler, Density Functional Theory Study of the Direct Conversion of Methane to Acetic Acid by $RhCl_3$, *Organometallics*, 2003, **22**, 3513–3525.
15 N. Kapur, J. Hyun, B. Shan, J. B. Nicholas and K. Cho, *Ab Initio* Study of CO Hydrogenation to Oxygenates on Reduced Rh Terraces and Stepped Surfaces, *J. Phys. Chem. C*, 2010, **114**, 10171–10182.
16 Y. M. Choi and P. Liu, Mechanism of Ethanol Synthesis from Syngas on Rh(111), *J. Am. Chem. Soc.*, 2009, **131**, 13054–13061.
17 Y. H. Zhao, K. J. Sun, X. F. Ma, J. X. Liu, D. P. Sun, H. Y. Su and W. X. Li, Carbon Chain Growth by Formyl Insertion on Rhodium and Cobalt Catalysts in Syngas Conversion, *Angew. Chem., Int. Ed.*, 2011, **50**, 5335–5338.
18 H. He, P. Zapol and L. A. Curtiss, A Theoretical Study of CO_2 Anions on Anatase (101) Surface, *J. Phys. Chem. C*, 2010, **114**, 21474–21481.
19 A. Hussain, D. Curulla Ferré, J. Gracia, B. E. Nieuwenhuys and J. W. Niemantsverdriet, DFT Study of CO and NO Adsorption on Low Index and Stepped Surfaces of Gold, *Surf. Sci.*, 2009, **603**, 2734–2741.
20 M. L. Yang, Y. A. Zhu, C. Fan, Z. J. Sui, D. Chen and X. G. Zhou, Density Functional Study of the Chemisorption of C_1, C_2 and C_3 Intermediates in Propane Dissociation on Pt(111), *J. Mol. Catal. A: Chem.*, 2010, **321**, 42–49.
21 R. C. Catapan, A. A. M. Oliveira, Y. Chen and D. G. Vlachos, DFT Study of the Water–Gas Shift Reaction and Coke Formation on Ni(111) and Ni(211) Surfaces, *J. Phys. Chem. C*, 2012, **116**, 20281–20291.
22 L. C. Grabow and M. Mavrikakis, Mechanism of Methanol Synthesis on Cu through CO_2 and CO Hydrogenation, *ACS Catal.*, 2011, **1**, 365–384.
23 M. Shishkin and T. Ziegler, Oxidation of H_2, CH_4, and CO Molecules at the Interface Between Nickel and Yttria-Stabilized Zirconia: A Theoretical Study Based on DFT, *J. Phys. Chem. C*, 2009, **113**, 21667–21678.
24 J. G. Wang, C. J. Liu, Y. P. Zhang and B. Eliasson, A DFT study of synthesis of acetic acid from methane and carbon dioxide, *Chem. Phys. Lett.*, 2003, **368**, 313–318.
25 R. G. Zhang, L. Z. Song, H. Y. Liu and B. J. Wang, The interaction mechanism of CO_2 with CH_3 and H on Cu(111) surface in synthesis of acetic acid from CH_4/CO_2: A DFT study, *Appl. Catal. A: Gen.*, 2012, **443–444**, 50–58.
26 R. G. Zhang, W. Huang and B. J. Wang, Thermodynamics of Direct Synthesis of Acetic Acid from CH_4 and CO_2 by a Two-step Isothermal Reaction Sequence on Co/Pd Catalysts, *Chin. J. Catal.*, 2008, **29**, 913–920.
27 M. M. Yang, X. H. Bao and W. X. Li, Density functional theory study of CH_x (x = 1–3) adsorption on clean and CO precovered Rh(111) surfaces, *J. Chem. Phys.*, 2007, **127**, 024705.
28 R. He, H. Kusaka, M. Mavrikakis and J. A. Dumesic, Microcalorimetric, Infrared Spectroscopic and DFT Studies of CO Adsorption on Rh and Rh–Te Catalysts, *J. Catal.*, 2003, **217**, 209–221.
29 M. Mavrikakis, J. Rempel, J. Greeley, L. B. Hansen and J. K. Nørskov, Atomic and Molecular Adsorption on Rh(111), *J. Chem. Phys.*, 2002, **117**, 6737–6744.
30 H. Xiao and D. Xie, A DFT Investigation of the Adsorption of Methyl on Rh(111), *Surf. Sci.*, 2004, **558**, 15–22.
31 B. S. Bunnik and G. J. Kramer, Energetics of Methane Dissociative Adsorption on Rh{111} from DFT Calculations, *J. Catal.*, 2006, **242**, 309–318.
32 P. Raybaud, M. Digne, R. Iftimie, W. Wellens, P. Euzen and H. Toulhoat, Morphology and Surface Properties of Boehmite (γ-AlOOH): A Density Functional Theory Study, *J. Catal.*, 2001, **201**, 236–246.

33 Z. J. Zuo, L. L. Sun, W. Huang, P. D. Han and Z. H. Li, Surface properties of copper in different solvent mother solutions: A density functional theory study, *Appl. Catal. A: Gen.*, 2010, **375**, 181–187.

34 G. Kresse and J. Furthmuller, Efficient Iterative Schemes for *Ab Initio* Total-energy Calculations Using a Plane-wave Basis Set, *Phys. Rev. B: Condens. Matter Mater. Phys.*, 1996, **54**, 11169–21118.

35 G. Kresse and J. Furthmuller, Efficiency of *Ab Initio* Total Energy Calculations for Metals and Semiconductors Using a Plane-wave Basis Set, *Comput. Mater. Sci.*, 1996, **6**, 15–50.

36 J. P. Perdew, J. A. Chevary, S. H. Vosko, K. A. Jackson, M. R. Pederson, D. J. Singh and C. Fiolhais, Atoms, Molecules, Solids, and Surfaces: Applications of the Generalized Gradient Approximation for Exchange and Correlation, *Phys. Rev. B: Condens. Matter Mater. Phys.*, 1992, **46**, 6671–6687.

37 P. E. Blöchl, Projector Augmented-wave Method, *Phys. Rev. B: Condens. Matter Mater. Phys.*, 1994, **50**, 17953–17979.

38 G. Kresse and D. Joubert, From ultrasoft pseudopotentials to the projector augmented-wave method, *Phys. Rev. B: Condens. Matter Mater. Phys.*, 1999, **59**, 1758–1775.

39 Y. H. Zhao, M. M. Yang, D. P. Sun, H. Y. Su, K. J. Sun, X. F. Ma, X. H. Bao and W. X. Li, Rh-Decorated Cu Alloy Catalyst for Improved C_2 Oxygenate Formation from Syngas, *J. Phys. Chem. C*, 2011, **115**, 18247–18256.

40 D. Sheppard, P. Xiao, W. Chemelewski, D. D. Johnson and G. Henkelman, A Generalized Solid-state Nudged Elastic Band Method, *J. Chem. Phys.*, 2012, **136**, 074103-1–074103-8.

41 D. Sheppard, R. Terrell and G. Henkelman, Optimization Methods for Finding Minimum Energy Paths, *J. Chem. Phys.*, 2008, **128**, 134106-1–134106-10.

42 G. Henkelman and H. Jónsson, A Dimer Method for Finding Saddle Points on High Dimensional Potential Surfaces Using only First Derivatives, *J. Chem. Phys.*, 1999, **111**, 7010–7022.

43 R. A. Olsen, G. J. Kroes, G. Henkelman, A. Arnaldsson and H. Jónsson, Comparison of Methods for Finding Saddle Points Without Knowledge of the Final States, *J. Chem. Phys.*, 2004, **121**, 9776–9792.

44 P. W. van Grootel, E. J. M. Hensen and R. A. van Santen, DFT Study on H_2O Activation by Stepped and Planar Rh Surfaces, *Surf. Sci.*, 2009, **603**, 3275–3281.

45 P. W. van Grootel, R. A. van Santen and E. J. M. Hensen, Methane Dissociation on High and Low Indices Rh Surfaces, *J. Phys. Chem. C*, 2011, **115**, 13027–13034.

46 M. Mavrikakis, M. Bäumer, H. J. Freund and J. K. Nørskov, Structure Sensitivity of CO Dissociation on Rh Surfaces, *Catal. Lett.*, 2002, **81**, 153–156.

47 W. M. H. Sachtler and M. Ichikawa, Catalytic Site Requirements for Elementary Steps in Syngas Conversion to Oxygenates over Promoted Rhodium, *J. Phys. Chem.*, 1986, **90**, 4752–4758.

48 M. Yamada, N. Koizumi, A. Miyazawa and T. Furukawa, Novel Catalytic Properties of Rh Sulfide for the Synthesis of Methanol from CO + H_2 in the Presence of H_2S, *Catal. Lett.*, 2002, **78**, 195–199.

49 H. Y. Luo, P. Z. Lin, S. B. Xie, H. W. Zhou, C. H. Xu, S. Y. Huang, L. W. Lin, D. B. Liang, P. L. Yin and Q. Xin, The role of Mn and Li promoters in supported rhodium catalysts in the formation of acetic acid and acetaldehyde, *J. Mol. Catal. A: Chem.*, 1997, **122**, 115–123.

50 W. M. Chen, Y. J. Ding, D. H. Jiang, T. Wang and H. Y. Luo, A selective synthesis of acetic acid from syngas over a novel Rh nanoparticles/nanosized SiO_2 catalysts, *Catal. Commun.*, 2006, **7**, 559–562.

51 R. G. Zhang, G. R. Wang and B. J. Wang, Insights into the mechanism of ethanol formation from syngas on Cu and an expanded prediction of improved Cu-based catalyst, *J. Catal.*, 2013, **305**, 238–255.

52 M. Li, W. Y. Guo, R. B. Jiang, L. M. Zhao, X. Q. Lu, H. Y. Zhu, D. L. Fu and H. H. Shan, Density Functional Study of Ethanol Decomposition on Rh(111), *J. Phys. Chem. C*, 2010, **114**, 21493–21503.

53 Y. M. Choi and P. Liu, Understanding of ethanol decomposition on Rh(111) from density functional theory and kinetic Monte Carlo simulations, *Catal. Today*, 2011, **165**, 64–70.

54 P. Liu and J. A. Rodriguez, Water–gas-shift reaction on metal nanoparticles and surfaces, *J. Chem. Phys.*, 2007, **126**, 164705.

55 P. Liu, A. Logadottir and J. K. Nørskov, Modeling the electro-oxidation of CO and H_2/CO on Pt, Ru, PtRu and Pt_3Sn, *Electrochim. Acta*, 2003, **48**, 3731–3742.

